Polymer 51 (2010) 1355–1362

Contents lists available at ScienceDirect

Polymer

journal homepage: www.elsevier.com/locate/polymer

Design and stabilization of block copolymer micelles via phenol–pyridine hydrogen-bonding interactions

Alaitz Ruiz de Luzuriaga [a], Iñaki García [a,c], David Mecerreyes [a], Agustin Etxeberria [b], José A. Pomposo [d,*]

[a] New Materials Department, CIDETEC – Centre for Electrochemical Technologies, Parque Tecnológico de San Sebastián, Paseo Miramón 196, Donostia-San Sebastián E 20009, Spain
[b] Departament of Polymer Science and Technology, Faculty of Chemistry and Polymat, UPV/EHU, P.O. Box 1072, E-20018 Donostia-San Sebastián, Spain
[c] CIC nanoGUNE Consolider, Paseo de Mikeletegui 56 E-20.009 – San Sebastián, Spain 20009 Donostia – San Sebastián, Spain
[d] Donostia International Physics Center, Paseo Manuel de Lardizabal 4, 20018 San Sebastián, Spain

ARTICLE INFO

Article history:
Received 21 September 2009
Received in revised form
14 January 2010
Accepted 15 January 2010
Available online 25 January 2010

Keywords:
Block copolymer
Micelles
Hydrogen bond

ABSTRACT

A new approach for the preparation of block copolymer micelles in non-selective solvent is introduced. Phenol–pyridine hydrogen-bonding interactions are used for the first time to prepare core–shell micelles in non-selective solvents using block copolymers and bifunctional low-molecular-weight hydrogen-bonding crosslinkers. Poly(styrene-*b*-4-vinylphenol)/Bis-pyridyl ethane and poly(styrene-*b*-4-vinylpyridine)/Bisphenol A were investigated as micelle formation due to phenol–pyridine hydrogen bond crosslinking. The influence of several factors such as temperature, concentration, solvent and pH in micellization–demicellization process was analyzed by Fourier transform infrared spectroscopy (FTIR), differential scanning calorimetry (DSC), dynamic light scattering (DLS) and atomic force microscopy (AFM). This method opens new possibilities to the generation of block copolymer micelles in non-selective solvents.

© 2010 Elsevier Ltd. All rights reserved.

1. Introduction

Micellization of block copolymers has attracted considerable attention due to their application in many research areas such as cosmetics, drug delivery, electronics, pollution control or separation technologies [1–6]. In most cases micellization of block copolymers takes place in selective solvents resulting in different morphologies such as spherical micelles, vesicles or wormlike aggregates, among others [7,8]. Recently, micelle formation of non-amphiphilic block copolymers in non-selective solvents in which both blocks are soluble has been reported [9]. In this case, block copolymers can form micelles due to non-covalent crosslinking [10,11] or chemical crosslinking [12,13] of one of the blocks. While amphiphilic block copolymers have a limitation in the molecular design, non-amphiphilic block copolymers have no dependence on solvent solubility [14]. Micellization of non-amphiphilic block copolymers has advantages over that of amphiphilic copolymers because it allows to choose appropriate additives to promote micellization, and hence to tailor the corresponding self-assembling driving force [15–20].

Recently, the concept of hydrogen-bonding complexation-induced micellization has been exploited to construct micelles from block copolymers in non-selective solvents. In a pioneering work, Yoshida and Kunugi [9] reported micellization of poly(styrene)-*block*-poly(4-vinylphenol) copolymers in dioxane, that is a good solvent for both blocks, by non-covalent hydrogen-bonding crosslinking in the presence of 1,4-butanediamine. Formation of thermoresponsive micellar complexes from poly(styrene-*b*-2-vinylpyridine) and poly(methacrylic acid) in dioxane [21] was further reported. The construction of polymeric micelles and hollow spheres in solution via specific intermolecular interactions has been recently reviewed by Chen and Jiang [22,23].

On the other hand, the strong hydrogen-bonding interaction between phenol- and pyridine-bearing polymers has been investigated by several groups. In low polar solvents, formation of an insoluble 1:1 complex upon mixing poly(vinylphenol) PVPh and poly(4-vinylpyridine) (PVPy) solutions was observed [24–26]. The two-dimensional cooperativity in the binding of PVPh to PVPy was studied using liquid and solid-state NMR and quantum mechanical calculations [27]. Complexation between poly(styrene-*co*-4-vinylphenol) and poly(styrene-*co*-4-vinylpyridine) in solution as well as the inter- and intrapolymer complexation in neat poly(4-vinylphenol-*b*-4-vinylpyridine) have been described [28]. Recently, hydrogen-bonding-directed layer-by-layer assembly of

* Corresponding author. Tel.: +34 943 01 53 68; fax: +34 943 01 56 00.
E-mail address: josetxo_pomposo@ehu.es (J.A. Pomposo).

0032-3861/$ – see front matter © 2010 Elsevier Ltd. All rights reserved.
doi:10.1016/j.polymer.2010.01.032

PVPh and PVPy into multilayer ultrathin films has been demonstrated [29].

In this work, phenol–pyridine hydrogen-bonding interactions are used for the first time to prepare core–shell micelles in non-selective solvents using block copolymers and bifunctional low-molecular-weight hydrogen-bonding crosslinkers. The micellar size and minimum crosslinker concentration to obtain micelles are determined by dynamic light scattering (DLS) measurements in different non-selective solvents. Also, strategies to stabilize the micelles to give core–shell nanoparticles are also described. To confirm the existence of core-crosslinked nanoparticles results from different techniques are combined such as Fourier transform infrared spectroscopy (FTIR), differential scanning calorimetry (DSC) and atomic force microscopy (AFM).

2. Experimental

2.1. Materials

Two block copolymers, Poly(styrene-*b*-4-vinylpyridine) (PS-*b*-PVPy) ($M_w/M_n = 1.09$, $M_{nPS} = 11{,}800$ g/mol, $M_{nPVPy} = 15{,}000$ g/mol) and Poly(styrene-*b*-4-vinylphenol) (PS-*b*-PVPh) ($M_w/M_n = 1.07$, $M_{nPS} = 7500$ g/mol, $M_{nPVPh} = 5000$ g/mol), were purchased from Polymer Source Inc. Bisphenol A (BPA), 1,2-Bis(4-pyridil)ethane (BPE) and all other reagents were purchased from Sigma–Aldrich and used without further purification.

2.2. Preparation of PS-b-PVPh/BPE and PS-b-PVPy/BPA micelles in 2-butanone

PS-*b*-PVPh (50 mg) (or PS-*b*-PVPy, 15 mg) was dissolved in 2-butanone (10 mL) for 24 h to form a molecularly dispersed solution. The resulting solution was passed through a 0.45 μm PTFE filter, injected into a cell and subjected to light scattering measurements at 20 °C. After the measurement, BPE (0.031 g) or BPA (0.018 g) was added to the PS-*b*-PVPh (or PS-*b*-PVPy) solution with stirring, allowing it to stabilize for 10 min at 20 °C before light scattering measurements. This procedure was repeated until disappearance of the unimer peak corresponding to the individual PS-*b*-PVPh (or PS-*b*-PVPy) chains was observed. The same procedure was employed for obtaining suspensions of PS-*b*-PVPh/BPE and PS-*b*-PVPy/BPA micelles in other solvents (THF, DMF).

2.3. Preparation of stabilized PS-b-PVPh/BPE and PS-b-PVPy/BPA nanoparticles

A suspension containing PS-*b*-PVPh/BPE (or PS-*b*-PVPh/BPA) micelles in 2-butanone was added dropwise to mildly stirred toluene that is a selective solvent for PS. After that, 2-butanone (b.p. 80 °C) was removed by distillation to obtain a suspension of core-stabilized nanoparticles in toluene. In order to remove the excess of BPE (or BPA), an extraction procedure with mild acid solution (or mild basic solution) was performed.

2.4. Measurement techniques

Particle size measurements were performed on a Dynamic Light Scattering (DLS) Beckman Coulter N5 Submicron Particle Size Analyzer at a scattering angle of 90°. All the samples used in the dynamic light scattering measurements were clarified by passing them through a 0.45 μm PTFE filter.

FTIR spectra were recorded at 25 °C on a Nicolet Avatar 360 spectrophotometer. All samples were cast directly onto KBr pellets. The spectra were taken with a 4 cm^{-1} resolution in a wavenumber range from 4000–400 cm^{-1}.

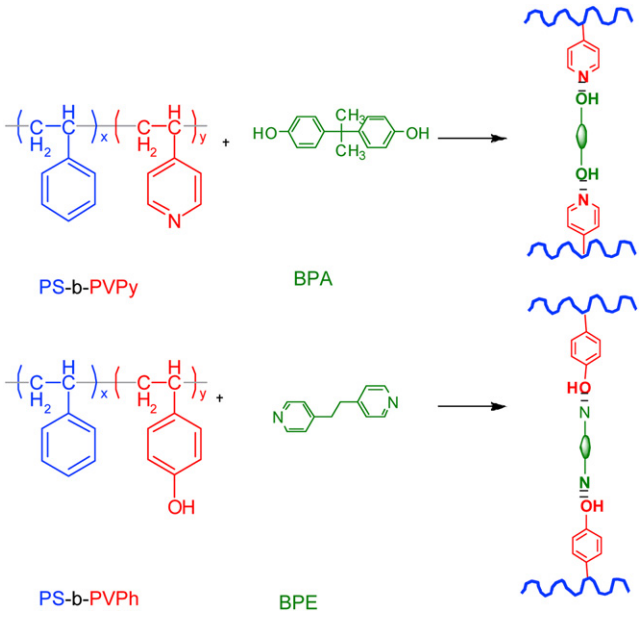

Scheme 1. Chemical structures of the materials used and micelle formation via hydrogen-bonding.

Thermal analysis was performed on a DSC instrument from Perkin Elmer (Pyris Diamond DSC) over a temperature range from 0 °C to 220 °C under Nitrogen. The glass transition temperature (T_g) was obtained as the inflection point of the heat flow step recorded at a scan rate of 20 °C/min. Solvent was removed in a rotary film evaporator and after that all samples were dried at 60 °C under vacuum for 48 h.

Atomic force microscopy (AFM) images of the samples were obtained in a tapping mode at room temperature using a scanning probe microscope (Molecular Imaging's PicoScan) equipped with a Nanosensors tips/cantilever having a resonance frequency of approximately 330 KHz and a spring constant of about 42 N/m with a tip nominal radius lower than 7 nm.

3. Results and discussion

3.1. Block copolymer micelles in non-selective solvents based on phenol–pyridine hydrogen-bonding interactions

Two block copolymers (PS-*b*-PVPy and PS-*b*-PVPh) were selected for micelle construction by mixing them with two complementary bifunctional low-molecular-weight hydrogen-bonding crosslinkers, BPA and BPE, respectively (see Scheme 1). Based on the hydrogen-bonding complexation-induced micellization concept, core–shell micelles should be formed by solving PS-*b*-PVPy and BPA (or PS-*b*-PVPh and BPE) in non-selective solvents at appropriate molar ratios. The driving force for micellization should be the well known phenol–pyridine hydrogen-bonding interaction (enthalpy of hydrogen bond formation about −7 Kcal/mol in apolar solvents) [30]. A certain competition for hydrogen-bonding formation from the solvent was expected since good solvents for PS-*b*-PVPy/BPA and PS-*b*-PVPh/BPE mixtures are in fact relatively polar ones (see Table 1). In this sense, it is well known that an insoluble 1:1 PVPh/PVPy complex cannot be obtained in DMF [31] due to the strong hydrogen-bonding competition from solvent molecules precluding complex formation. In the present study, the influence of solvent quality, temperature and pH on PS-*b*-PVPy/BPA and PS-*b*-PVPh/BPE micelle formation is addressed.

Table 1
Solubility of PS-*b*-PVPy, BPE, PS-*b*-PVPy and BPA in several solvents at room temperature.

Solvent	PS-*b*-PVPh	BPE	PS-*b*-PVPy	BPA
$CHCl_3$	+	−	+	−
THF	+	+	+	+
Butanone	+	+	+	+
Acetone	−	+	−	+
DMF	+	+	+	+
Toluene	−	−	−	−

Table 2
Effect of the solvent on the micellization process for PS-*b*-PVPh/BPE and PS-*b*-PVPy/BPA systems.

Solvent	PS-*b*-PVPh [5×10^{-3} M]/BPE		PS-*b*-PVPy [1.5×10^{-3} M]/BPA	
	BPE/PVPh[a]	Micelle size	BPA/PVPy[a]	Micelle size
Butanone	8	30 nm	3	32 nm
THF	18	18 nm	15[b]	18 nm[b]
DMF	–	–	–	–

[a] Given as the molar ratio of bifunctional hydrogen-bonding crosslinker to block copolymer.
[b] PS-*b*-PVPy [5×10^{-3} M]/BPA.

First, the effect of the solvent quality in the unimers-to-micelles transition for the PS-*b*-PVPy/BPA and PS-*b*-PVPh/BPE systems is summarized in Table 2. It is well known that hydrogen-bonding formation is dependent on solvent quality since complexation between complementary phenol and pyridine functional groups in these systems is a result of the competition between pyridine–BPA (or phenol–BPE) interactions and pyridine-solvent (or phenol-solvent) interactions, respectively. PS-*b*-PVPy/BPA and PS-*b*-PVPh/BPE micellation takes place in 2-butanone and THF, the former requiring a lower crosslinker concentration than the later, but does not take place in DMF which is a strong proton-accepting solvent. These results are in good agreement with the hydrogen-bonding ability of these solvents: DMF > THF > 2-butanone.

The evolution of the micellization process for the PS-*b*-PVPh/BPE/butanone system at 20 °C as determined by DLS measurements upon increasing the [BPE]/[PVPh] molar ratio is shown in Fig. 1A. In absence of hydrogen-bonding crosslinking BPE molecules, the PS-*b*-PVPh chains [5×10^{-3} g/mL] are in the form of unimers with a hydrodynamic diameter of 4.4 ± 0.5 nm. A transition from unimers to micelles is clearly observed upon progressive BPE addition, leading to well-defined aggregates (see Scheme 2). As illustrated in Fig. 1B, micelle formation takes place at [BPE]/[PVPh] ~ 8 M ratio and the resulting micelles show a hydrodynamic diameter of $\sim 30 \pm 5$ nm. Fig. 1C shows the unimers-to-micelles transition for the PS-*b*-PVPy/BPA/butanone system. In this case, the individual PS-*b*-PVPy chains [1.5×10^{-3} g/mL] present a hydrodynamic diamenter of 4.4 ± 0.5 nm. In Fig. 1D micelle formation is observed at [BPA]/[PVPy] ~ 3 M ratio leading to micelles with a hydrodynamic diameter of $\sim 32 \pm 5$ nm. The differences observed in the [crosslinker]/[crosslinkable units] molar ratio needed to obtain well-defined aggregates in the PS-*b*-PVPy/BPA and PS-*b*-PVPh/BPE systems mainly arise from both differences in concentration and block copolymer chain lengths (*i.e.* copolymers with long crosslinkable blocks need less crosslinker molecules for micellization).

Next, the effect of temperature on the phenol–pyridine hydrogen-bonding micellization process was investigated for both systems. The thermostability of the micelles was determined by DLS analysis as illustrated in Fig. 2A and B. When temperature was increased a decrease in the hydrodynamic diameter was observed since the strength of the hydrogen-bonding interactions weakens with temperature. The decrease of the hydrodynamic diameter on heating can be attributed to the release of crosslinker molecules from the micellar core to the solution and the concomitant increase in the proportion of unimers at higher temperatures.

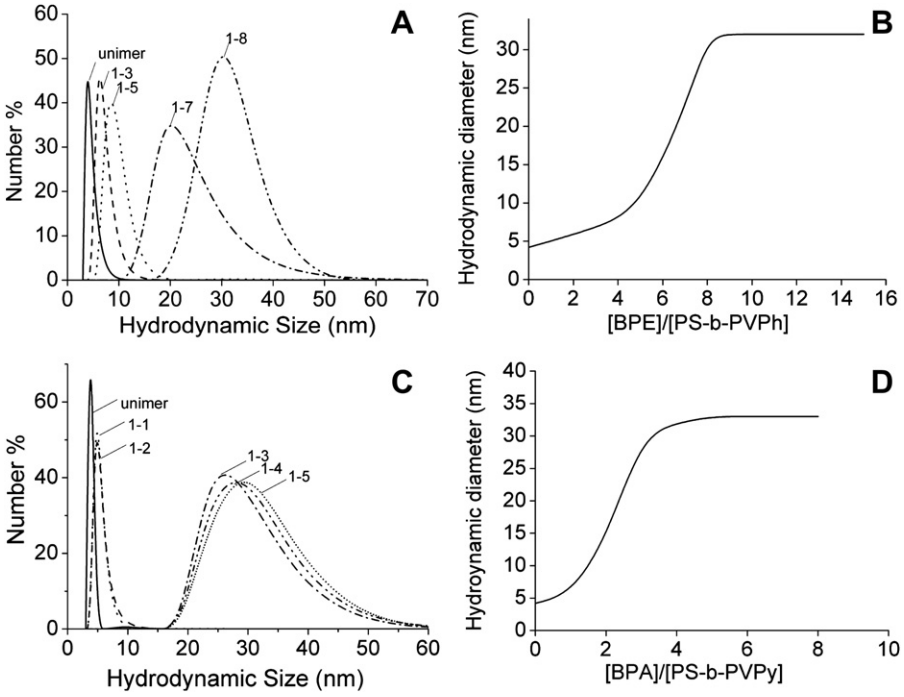

Fig. 1. DLS measurements of evolution of the micellization process for the PS-*b*-PVPh/BPE/Butanone system (A) at 20 °C upon increasing [BPE/PVPh] molar ratio. (B) Shows the variation in the hydrodynamic diameter versus [BPE/PVPh] molar ratio. DLS measurements of evolution of the micellization process for the PS-*b*-PVPy/BPA/Butanone system (C) at 20 °C upon increasing [BPA/PVPy] molar ratio. (D) Shows the variation in the hydrodynamic diameter versus [BPA/PVPy] molar ratio.

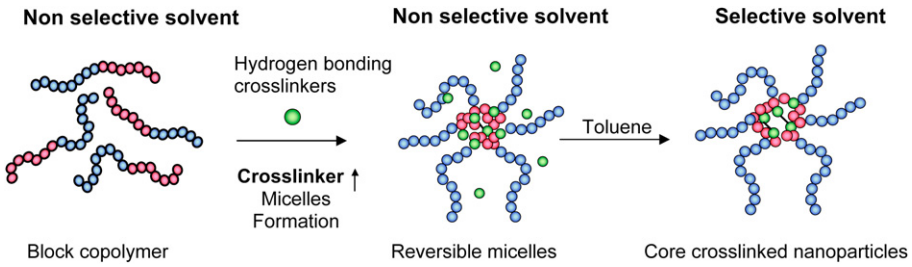

Scheme 2. Micelles formation in non-selective solvent and core-crosslinked nanoparticles.

Finally, Fig. 3A and B shows DLS measurements of the PS-*b*-PVPh/BPE and PS-*b*-PVPy/BPA systems after addition of acetic acid or 4-(Dimethylamino)pyridine (DMAP), respectively. Demicellization was observed when acetic acid and DMAP were added to both micelle suspensions due to the competition between acetic acid or DMAP and bifunctional crosslinker molecules.

Interestingly, it was found that dilution brokes both the PS-*b*-PVPh/BPE and PS-*b*-PVPy/BPA micelles to give back the corresponding unimers, demonstrating the equilibrium existing between unimers and micelles as a function of solvent concentration and the reversible nature of non-crosslinked micelles.

3.2. From reversible micelles to stabilized core–shell nanoparticles based on phenol–pyridine hydrogen-bonding interactions

Stabilized core–shell nanoparticles were obtained by phase inversion followed by simple extraction of the excess of crosslinker molecules in solution. Toluene was employed as non-solvent for PVPy, BPA, PVPh and BPE but selective solvent for PS (see Table 1). Hence, when PS-*b*-PVPy/BPA/2-butanone or PS-*b*-PVPh/BPE/2-butanone micelle suspensions were added dropwise to toluene no precipitation was observed due to the presence of the soluble PS blocks in the external shell of the micelles. When 2-butanone and the crosslinker excess were removed by distillation and extraction, respectively, a suspension of stabilized core–shell nanoparticles resulted.

First, the obtention of stabilized core–shell nanoparticles was investigated by FTIR measurements. In this sense, Fig. 4A and B show the FTIR spectra of the PS-*b*-PVPh/BPE nanoparticles. Fig. 4A shows the hydroxyl region of pure PS-*b*-PVPh block copolymer, pure BPE and core–shell PS-*b*-PVPh/BPE nanoparticles. Pure PS-*b*-PVPh copolymer shows two bands in this region arising from the PVPh block: a peak corresponding to free hydroxyl groups located at 3525 cm^{-1} and a broad band centred at 3350 cm^{-1} corresponding to a distribution of hydrogen bonded hydroxyl groups [32]. The BPE bifunctional crosslinker shows no absorption band in this region. For the core–shell PS-*b*-PVPh/BPE nanoparticles, the intensity of free hydroxyl groups disappears, suggesting that hydroxyl groups are now hydrogen bonded to pyridine –N═ groups

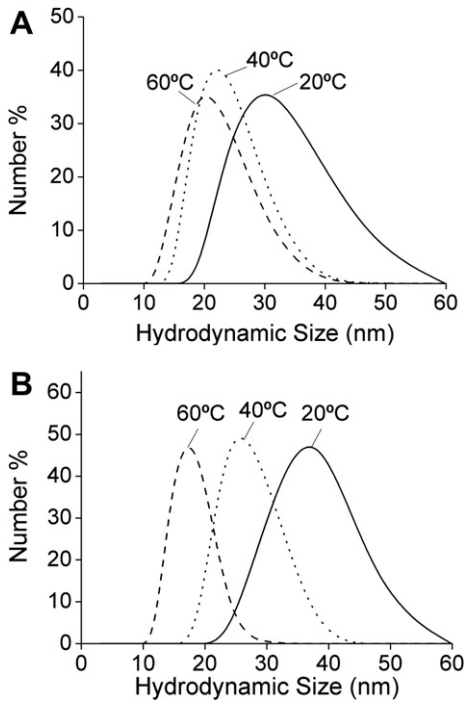

Fig. 2. A). DLS measurements of number distribution of PS-*b*-PVPh + BPE micelles in butanone at different temperatures. (B). DLS measurements of number distribution of PS-*b*-PVPy + BPA micelles in butanone at different temperatures.

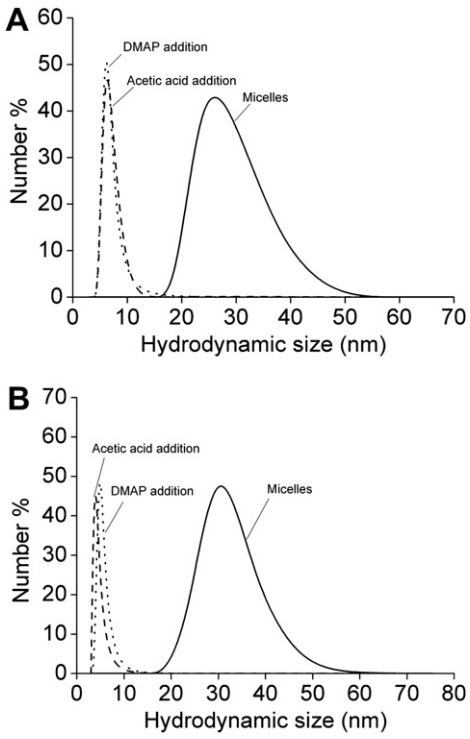

Fig. 3. A). DLS measurements before and after addition of acetic acid and DMAP PS-*b*-PVPh + BPE micelles solution. (B). DLS measurements before and after addition of acetic acid and DMAP PS-*b*-PVPy + BPA micelles solution.

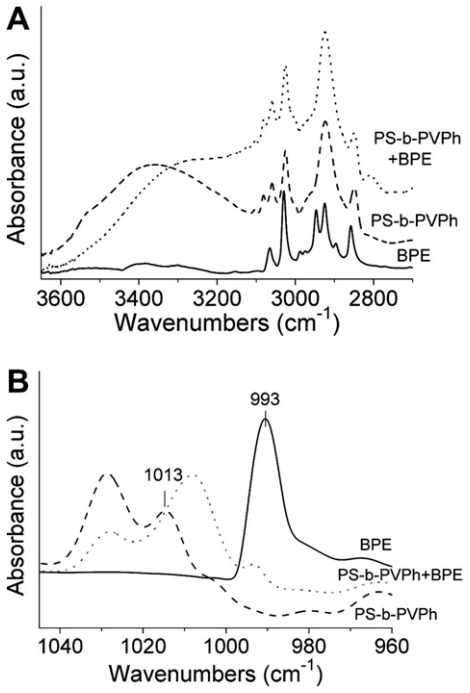

Fig. 4. A). Comparative FTIR spectra, of the hydroxyl region of PS-*b*-PVPh, BPE and PS-*b*-PVPh + BPE complex. (B). Comparative FTIR spectra, from 960 to 1040 cm^{-1} corresponding to the pyridine ring stretching modes of PS-*b*-PVPh, BPE and PS-*b*-PVPh + BPE complex.

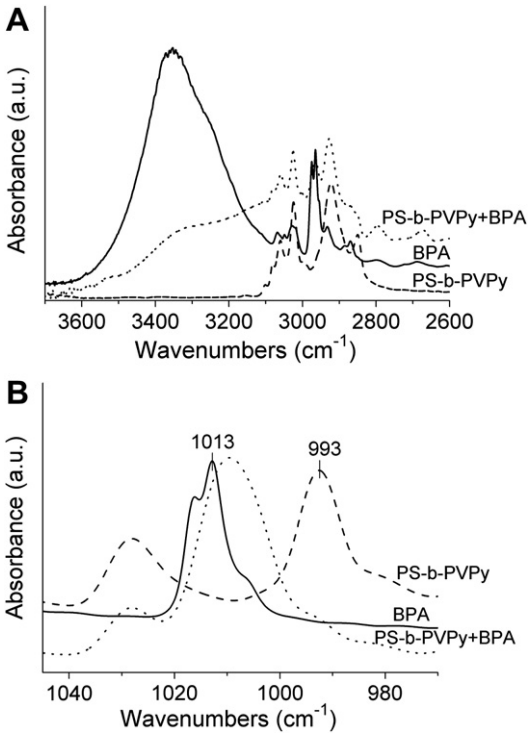

Fig. 5. A). Comparative FTIR spectra, of the hydroxyl region of PS-*b*-PVPy, BPA and PS-*b*-PVPy + BPA complex. (B). Comparative FTIR spectra, from 970 to 1040 cm^{-1} corresponding to the pyridine ring stretching modes of PS-*b*-PVPy, BPA and PS-*b*-PVPy + BPA complex.

from BPE. In Fig. 4B the FTIR spectrum from 960 to 1040 cm^{-1} corresponding to the pyridine ring stretching modes is shown. Pure BPE shows a characteristic band at 993 cm^{-1} corresponding to BPE ring absorption [33,34]. On the contrary, the PS-*b*-PVPh block copolymer shows no absorption peak at 993 cm^{-1}, but exhibits an absorption band at 1013 cm^{-1}. The core–shell PS-*b*-PVPh/BPE nanoparticles show a new band at 1005 cm^{-1} which is assigned to hydrogen bonded pyridine rings with phenol groups [29]. In the same way, Fig. 5A and B illustrate the FTIR spectra of core–shell PS-*b*-PVPy/BPA nanoparticles. Fig. 5A shows the FTIR region were the hydroxyl group bands are observed. Neat BPA shows a single band centred at 3350 cm^{-1} corresponding to hydrogen bonded hydroxyl-hydroxyl groups. The PS-*b*-PVPy block copolymer shows no absorption peak in this region. The core–shell PS-*b*-PVPy/BPA nanoparticles show a very broad band spanning from 3100 to 3600 cm^{-1} that includes the absorption from hydroxyl groups of BPA hydrogen bonded to pyridine units of the PS-*b*-PVPy copolymer (*ca.* 3125 cm^{-1}) [29]. In Fig. 5B the infrared spectra in the range 970–1040 cm^{-1} corresponding to the pyridine ring stretching modes is shown. The pure PS-*b*-PVPy copolymer shows a characteristic band at 993 cm^{-1} arising from pyridine ring absorption [33,34]. Neat BPA shows no absorption at 993 cm^{-1} but exhibits an absorption peak at 1013 cm^{-1}. The core–shell PS-*b*-PVPy/BPA nanoparticles show a new band at 1008 cm^{-1} which can be assigned to hydrogen bonded pyridine–phenol groups.

Next, differential thermal analysis (DSC) measurements were performed to confirm the obtention of stabilized core–shell nanoparticles (Figs. 6 and 7). As can be observed in Fig. 6, the pure PS-*b*-PVPh block copolymer shows two glass transition temperatures arising from the PS block (80 °C) and the PVPh block (150 °C). The core–shell PS-*b*-PVPh/BPE nanoparticles also show two glass transition temperatures: one at 80 °C that can be clearly assigned to

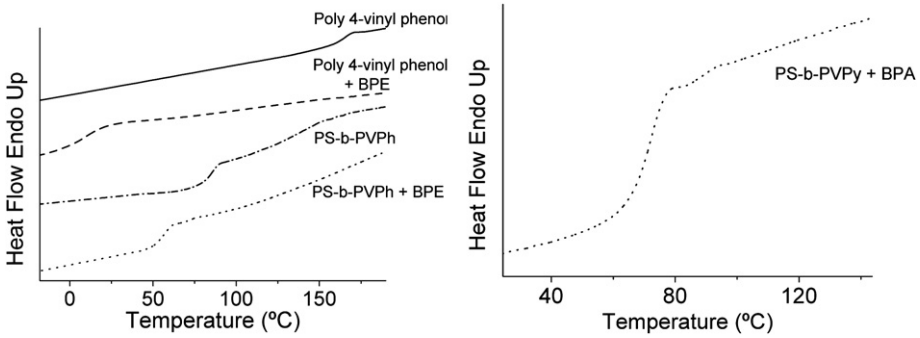

Fig. 6. Comparative DSC heat flow curves of poly 4-vinylphenol homopolymer (straight line), poly 4-vinylphenol + BPE mixture (dashed line), PS-*b*-PVPh block copolymer (Dot–dashed line) and PS-*b*-PVPh + BPE core-crosslinked nanoparticles (Doted line) (left). Zoom DSC heat flow curve of PS-*b*-PVPh + BPE core-crosslinked nanoparticles (right).

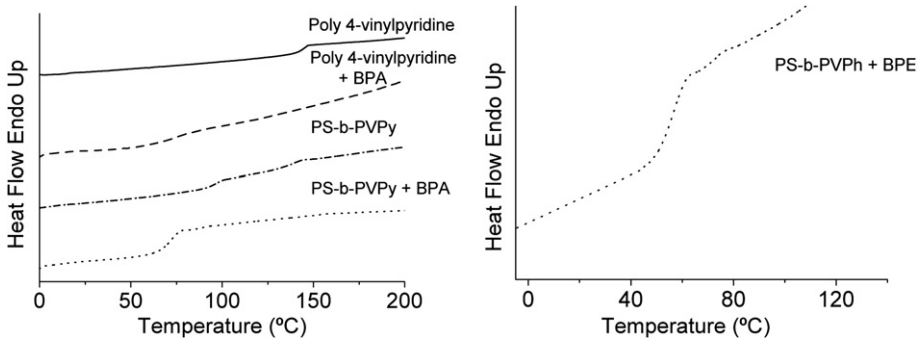

Fig. 7. Comparative DSC heat flow curves of poly 4-vinylpyridine homopolymer (straight line), poly 4-vinylpyridine + BPA mixture (dashed line), PS-*b*-PVPy block copolymer (Dot–dashed line) and PS-*b*-PVPy + BPA core-crosslinked nanoparticles (Doted line) (left). Zoom DSC heat flow curve of PS-*b*-PVPy + BPA core-crosslinked nanoparticles (right).

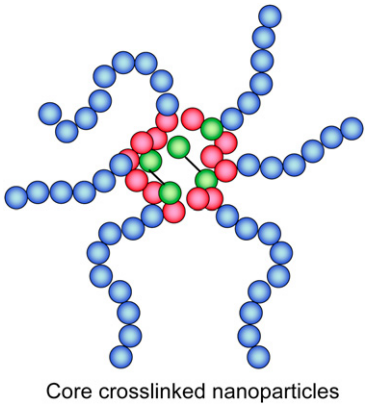

Scheme 3. Free volume increase in the core of the nanoparticle.

the PS shell and other at 50 °C that we tentatively assigned to the PVPh–BPE hydrogen bonded core. To confirm this assignment, a new experiment was performed which consists on recording the DSC thermogram of a PVPh homopolymer/BPE blend and compare it to that of neat PVPh. As illustrated in Fig. 6, PVPh homopolymer shows a single glass transition temperature at 155 °C whereas the PVPh homopolymer/BPE blend shows a single glass transition temperature at 15 °C (a large T_g depression of 100 °C). A similar behaviour was observed for stabilized core–shell PS-*b*-PVPy/BPA nanoparticles. The thermograms of the pure PS-*b*-PVPy copolymer and the core–shell PS-*b*-PVPy/BPA nanoparticles are illustrated in Fig. 7. As is expected, the PS-*b*-PVPy copolymer shows two glass transition temperatures: one at 95 °C, which corresponds to the PS blocks, and other at 140 °C, which corresponds to the PVPy ones. The stabilized core–shell PS-*b*-PVPy/BPA nanoparticles present two T_gs at 80 °C and 65 °C, respectively. Hence, a significant glass transition temperature decrease (about 80 °C) is also observed when compared to the T_g of the neat PVPy blocks due to the presence of the bifunctional crosslinker molecules in the nanoparticle core. A similar glass transition depression was found for model PVPy + BPA blends. In general, these results are in agreement with those observed upon blending PVPy and pentadecylphenol [35] pointing to a neat free volume increase and thus to a significant mobility enhancement at lower temperatures (see Scheme 3).

Finally, the size of the stabilized core–shell PS-*b*-PVPy/BPA and PS-*b*-PVPh/BPE nanoparticles was determined by two complementary techniques, such as DLS and AFM. It is worth noticing that a variety of factors should be taken account when DLS and AFM measurements are compared [36–39] such as broadening features arising from the finite radius of the AFM tip, the effect of carrying out the measurements without solvent or the inability of the AFM technique to probe voids that might exist between the micelles themselves leading to sample deformation. In this sense, Fig. 8A and Fig. 8B show DLS results corresponding to the PS-*b*-PVPh/BPE and PS-*b*-PVPy/BPA nanoparticles in toluene. The resulting nanoparticle sizes were 39 ± 5 nm and 40 ± 3 nm, respectively. These results are according to intrinsic structure of nanoparticles, as it was expected PS-*b*-PVPy/BPA nanoparticles has bigger diameter than PS-*b*-PVPh/BPE due to polymerization degree of PS-*b*-PVPy is larger than PS-*b*-PVPh. The corresponding height and phase AFM images are illustrated in Figs. 9 and 10 where the nanoparticle morphology is observed. By analyzing the height profile, the averaged diameter of the PS-*b*-PVPh/BPE and PS-*b*-PVPy/BPA

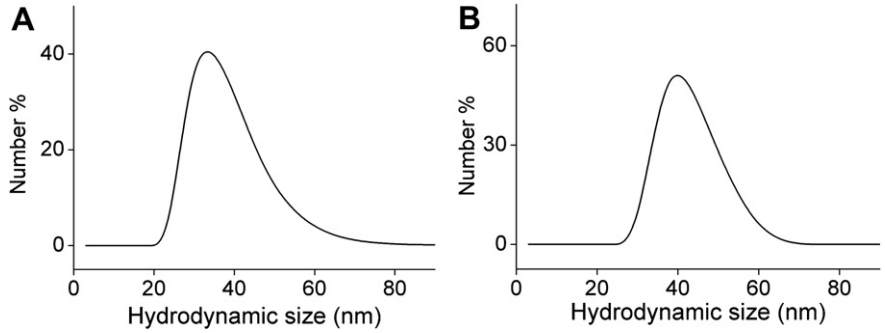

Fig. 8. (A) DLS measurements of number distribution of PS-*b*-PVPh + BPE nanoparticles in Toluene. (B) DLS measurements of number distribution of PS-*b*-PVPy + BPA nanoparticles in Toluene.

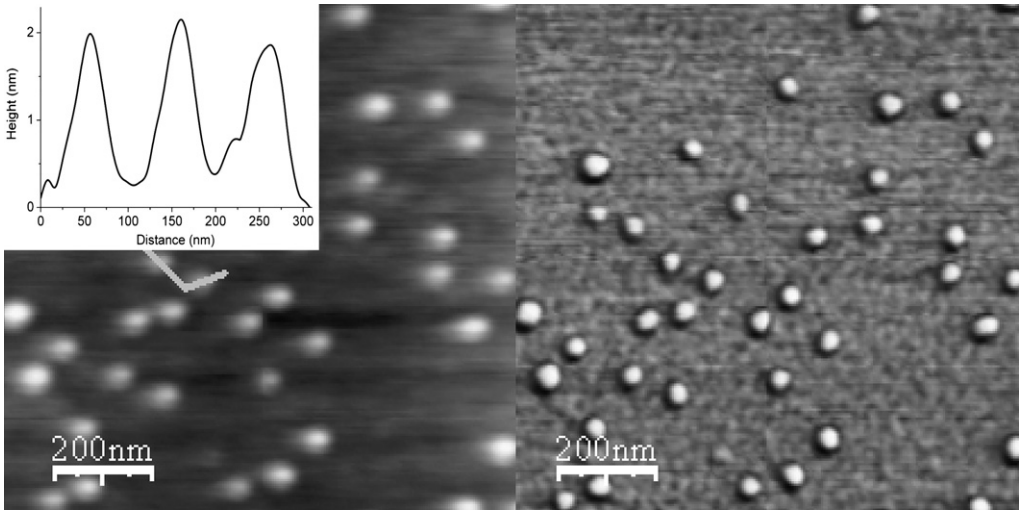

Fig. 9. Height (left) and phase (right) AFM images and height and phase profiles of PS-*b*-PVPh + BPE nanoparticles (bottom).

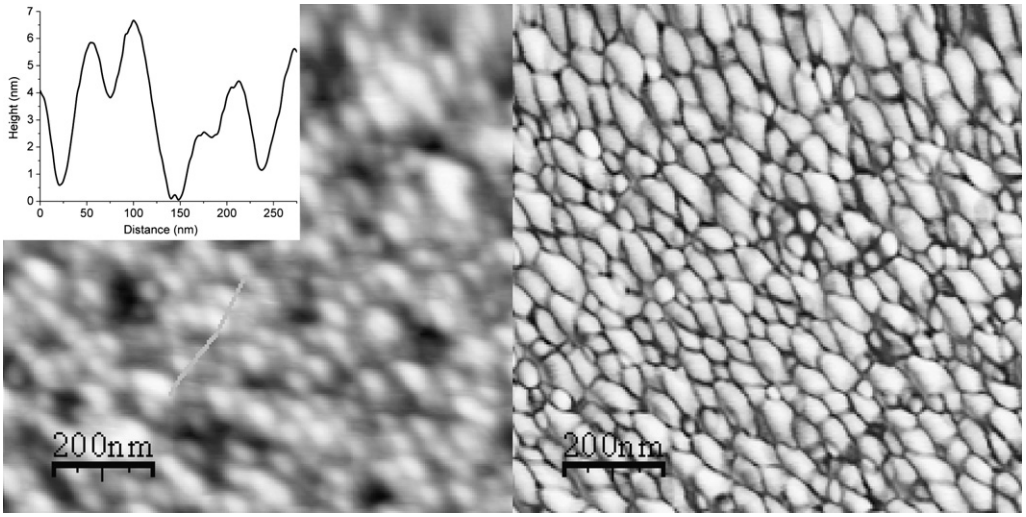

Fig. 10. Height (left) and phase (right) AFM images and height and phase profiles of self-assembled PS-*b*-PVPy + BPA nanoparticles (bottom).

nanoparticles is very similar in both cases (*ca.* 39 nm) in good agreement with the DLS results.

4. Conclusions

A new way to prepared polymeric micelles in non-selective solvent has been proposed. We have studied the spontaneous formation of poly(styrene-*b*-4-vinylphenol) and poly(styrene-*b*-4-vinylpyridine) micelles in non-selective solvent by addition of a low-molecular-weight hydrogen-bonging crosslinker as bis-pyridyl ethane and Bisphenol A, respectively. This method represents a fundamentally different mechanism for micelles formation due to micelles were prepared by addition of hydrogen-bonging crosslinker as difference of classic method where micelles are formed using a selective solvent to a block of block copolymer.

DLS was used to study the associative behaviour of systems in butanone that is non-selective solvent, as function of crosslinker and block copolymer molar ratio, temperature, pH and concentration. In order to obtain micelles [BPE]/[PVPh]∼8 and [BPA]/[PVPy]∼3 M ratio between crosslinker and block copolymer is necessary. As consequence of increment of temperature, sizes of micelles decrease because there is a relaxation of crosslinker molecules from the micellar core to the solution and the concomitant increase in the proportion of unimers at higher temperatures. When acetic acid or DMAP were added to suspensions demicellization was observed due to the competition between acetic acid or DMAP and bifunctional crosslinker molecules. Moreover, dilution of systems provokes demicellization.

FTIR allow to corroborate phenol–pyridine hydrogen bond in stabilized core–shell nanoparticles. Moreover, core–shell nanoparticles were analyzed by DSC. A decrease of T_g of core of nanoparticles due to free volume increment could be observed. Finally, size and morphology of nanoparticles was analyzed by two complementary techniques that shown a good correlation, as DLS and AFM.

Acknowledgements

The present work was supported by this work was supported by the Basque Government through i-Nanogune ETORTEK project and the Spanish Ministry of Science and Education: Consolider Project NANOGUNE CSD2006-0003.

References

[1] Zhu J, Yu H, Jiang W. Macromolecules 2005;38:7492–501.
[2] Massey J, Power KN, Manners I, Winnik MA. J Am Chem Soc 1998;120:9533–40.
[3] Kataoka K, Harada A, Nagasaki Y. Adv Drug Deliv Rev 2001;47:113–31.
[4] Savic R, Luo LB, Eisenberg A. Science 2003;300:615–8.
[5] Rösler A, Vandermeulen GWM, Klok HA. Adv Drug Deliv Rev 2001;53:95–108.
[6] Förster S, Antonietti M. Adv Mater 1998;10:195–217.
[7] (a) Zhang LF, Eisenberg A. Science 1995;268:1728–31;
(b) Zhang LF, Eisenberg A. Science 1996;272:1777–9;
(c) Jenekhe SA, Chen XL. Science 1998;279:1903–7;
(d) Discher BM, Won YY, Ege DS, Lee JCM, Bates FS, Discher DE, et al. Science 1999;284:11431146;
(e) Jain S, Bates FS. Science 2003;300:460–4;
(f) Cornelissen JJLM, Fischer M, Sommerdijk NJM, Nolte RJM. Science 1998;280:1427–30.
[8] (a) Stewart S, Liu GJ. Angew Chem Int Ed 2000;39:340–4;
(b) Ma QG, Remsen EE, Clark CG, Kowalewski T, Wooley KL. Proc Natl Acad Sci U S A 2002;99:5058–63.
[9] Yoshida E, Kunugi S. J Polym Sci Part A Polym Chem 2002;40:3063–7.
[10] Yoshida E, Kunugi S. Macromolecules 2002;35:6665–9.
[11] Thibault RJ, Hotchkiss PJ, Gray M, Rotello VM. J Am Chem Soc 2003;125:11249–52.
[12] Chen DY, Peng HS, Jiang M. Macromolecules 2003;36:2576–8.
[13] Ximei Y, Chen DY, Jiang M. Macromolecules 2004;37:4211–7.
[14] Yoshida E, Terada Y. Colloid Polym Sci 2005;283:1190–6.
[15] Bronstein LM, Sidorov SN, Valetsky PM. Langmuir 1999;15:6256–62.
[16] Liu S, Zhang G, Jiang M. Polymer 1999;40:5449–53.
[17] Gohy JF, Varshney SK, Jerome R. Macromolecules 2001;34:3361–6.
[18] Chernyshov DM, Bronstein LM, Boerner H, Berton B, Antonietti M. Chem Mater 2000;12:114–21.
[19] Liu S, Zhu H, Zha H, Jiang M, Wu C. Langmuir 2000;16:3712–7.
[20] Harada A, Kataoka K. Macromolecules 1995;28:5294–9.
[21] Topouza D, Orfanou K, Pispas S. J Polym Sci Part A Polym Chem 2004;42:6230–7.
[22] Duan H, Chen D, Jiang M, Gan W, Li S, Wang M, et al. J Am Chem Soc 2001;123:12097–8.
[23] Chen D, Jiang M. Acc Chem Res 2005;38:494–502.
[24] Dai J, Goh SH, Lee SY, Siow KS. Polym J 1994;26:905–11.
[25] Xiang ML, Jiang M, Zhang YB, Wu C, Feng LX. Macromolecules 1997;30:2313–9.
[26] Zhang YB, Xiang ML, Jiang M, Wu C. Macromolecules 1997;30:6084–9.
[27] Kriz J, Dybal J, Brus J. J Phys Chem B 2006;110:18338–46.
[28] Luo S, Liu S, Xu J, Liu H, Zhu Z, Jiang M, et al. Macromolecules 2006;39:4517–25.
[29] Zhang H, Wang Z, Zhang Y, Zhang X. Langmuir 2004;20:9366–70.
[30] Spencer JN, Andresky JC, Grushow A, Naghdi J, Patti LM, Trader JF. J Phys Chem 1987;91:1673–4.
[31] Zhang S, Painter PC, Runt J. Macromolecules 2004;37:2636–42.
[32] Kuo SW, Tung PH, Chang FC. Macromolecules 2006;39:9388–95.
[33] Ruokolainen J, Brinke G, Ikkala O. Macromolecules 1996;29:3409–15.
[34] Ruokolainen J, Tanner J, Ikkala O. Macromolecules 1998;31:3532–6.
[35] (a) Wit J, Ekenstein GA, Polushkin E, Kvashnina K, Bras W, Ikkala O, et al. Macromolecules 2008;41:4200–4;
(b) Luyten MC, Ekenstein GA, Brinke GT. Macromolecules 1999;32:4404–10;
(c) Brandys FA, Bazuin CG. Chem Mater 1996;8:83–92;
(d) Zoelen WV, Ekenstein GA, Ikkala O, Brinke GT. Macromolecules 2006;39:6574–9;
(e) Valkama S, Ruotsalainen T, Nyka1nen A, Laiho A, Kosonen H, Brinke GT, et al. Macromolecules 2006;39:9327–36.
[36] Zhang J, Chen P, Sun C, Hu X. Appl Catal A 2004;266:49–54.
[37] Vesenka J, Manne S, Giberson R, Marsh T, Henderson E. Biophys J 1993;65:992–7.
[38] Fun J, Feng X, Han Y, Pan C, Yang Y, Li B. Macromol Rapid Commun 2003;24:487–91.
[39] La Rue I, Adam M, da Silva M, Sheiko SS, Rubinstein M. Macromolecules 2004;37:5002–5.